Modeling Flow and Transport in Unsaturated Fractured Rock:

An Evaluation of the Continuum Approach

Hui-Hai Liu, Charles B. Haukwa, C. Fredrik Ahlers, Gudmundur S. Bodvarsson, Alan L. Flint[a], and William B. Guertal[a]

Earth Science Division
Lawrence Berkeley National Laboratory
University of California, Berkeley
California

[a]U.S. Geological Survey
Sacramento, California

Submitted to *Journal of Contaminant Hydrology* for Publication

Abstract

Because the continuum approach is relatively simple and straightforward to implement, it has been commonly used in modeling flow and transport in unsaturated fractured rock. However, the usefulness of this approach can be questioned in terms of its adequacy for representing fingering flow and transport in unsaturated fractured rock. The continuum approach thus needs to be evaluated carefully by comparing simulation results with field observations directly related to unsaturated flow and transport processes. This paper reports on such an evaluation, based on a combination of model calibration and prediction, using data from an infiltration test carried out in a densely fractured rock within the unsaturated zone of Yucca Mountain, Nevada. Comparisons between experimental and modeling results show that the continuum approach may be able to capture important features of flow and transport processes observed from the test. The modeling results also show that matrix diffusion may have a significant effect on the overall transport behavior in unsaturated fractured rocks, which can be used to estimate effective fracture-matrix interface areas based on tracer transport data. While more theoretical, numerical, and experimental studies are needed to provide a conclusive evaluation, this study suggests that the continuum approach is useful for modeling flow and transport in unsaturated, densely fractured rock.

Keywords: Unsaturated flow; Model calibration; Seepage; Matrix diffusion

1. Introduction

Flow and transport in unsaturated fractured rock are generally complicated, owing to the complexity of fracture-matrix interaction mechanisms, distinct differences in hydraulic properties between fractures and the matrix, and nonlinearity involved in unsaturated flow. Several approaches are available for modeling flow and transport in unsaturated fractured rock (Bear et al.,1993; National Research Council, 1996, 2001). Because the continuum approach is relatively simple and straightforward to implement, it has been commonly used in modeling flow and transport in unsaturated fractured rocks.

In the continuum approach, connected fractures and rock matrix are viewed as two or more overlapped, interacting continua. In other words, at a "point," two or more continua are considered to co-exist. In this case, continuum mechanics formulations, such as those used for porous media, can be used to describe flow and transport in each continuum. Coupling of processes between different continua is determined by their interaction mechanisms at a subgrid scale.

However, fundamental concerns regarding the usefulness of the continuum approach remains, especially about its adequacy for representing gravity-driven fingering flow and transport, resulting from subsurface heterogeneities and nonlinearity involved in unsaturated flow (Glass et al., 1996; Pruess, 1999; Pruess et al., 1999; Liu et al., 1998). Several authors (Glass et al., 1996; Pruess, 1999; Pruess et al., 1999) have suggested that the usefulness of the continuum approach needs to be carefully investigated for modeling flow and transport in unsaturated fractured rock. Given the complexities of the flow and transport processes, a direct comparison between numerical simulations (based on the

continuum approach) and field experimental observations would be a useful and relatively simple way to evaluate the validity of the approach (Pruess et al., 1999).

Field-scale experimental data of flow and transport through unsaturated fractured rock, obtained under controlled conditions, are very limited. However, a field-scale experiment of this kind was recently conducted at the Yucca Mountain site in an effort to improve our understanding of flow and transport processes there. This paper reports on the comparison between simulation results, obtained based on the continuum approach, and these experimental observations. The comparison shows that the continuum approach may be able to capture important features of flow and transport in unsaturated fractured rock.

2. Infiltration Test at the Yucca Mountain Site

An infiltration test was conducted at the Yucca Mountain site by the U.S. Geological Survey. The test site is located near the North Portal of the Exploratory Studies Facility (ESF), an underground tunnel constructed for characterizing the site. An alcove (underground opening) of the ESF, about 30 m below the ground surface, was constructed for collecting seepage water originating from the infiltration plot located at the ground surface. The alcove is about 5.5 m high and 5.8 m wide. Rocks between the ground surface and the alcove are intensely fractured. A bulkhead has been installed near the face of the alcove to isolate the end of the alcove from the ESF. The bulkhead is intended to raise the relative humidity at the end of the alcove and reduce evaporation from the wall of the alcove. This should allow observation of the wetting front arrival through observation of dripping from the alcove ceiling and walls.

During the infiltration test, water was applied at specific rates less than the fracture saturated hydraulic conductivity from the ground surface directly above the end of the alcove. The size of the infiltration plot was 7.9 m x 10.6 m. An irrigation drip tubing, with 490 drippers uniformly distributed within the infiltration plot, was used for applying water. Figure 1 shows applied infiltration rate as a function of time. The infiltration test started at time t = 0 (March 9, 1998) and consisted of two phases. Infiltration rates in Phase I exhibited a greater degree of temporal variability than those in Phase II. The temporal variability of infiltration rate is expected to result in complicated time-dependent flow behavior in the rock. Use of this temporal variability was partially motivated by a conceptual idea that, under ambient conditions, transient flow occurs in the test rock (Bodvarsson et al., 2001). During the late stage of Phase II, a tracer, bromide, was introduced into the infiltrating water by mixing the tracer with water in a tank that supplied water for the surface infiltration. Total seepage into the alcove was collected using a collection system consisting of 432 relatively small containers (trays) placed just below the ceiling of the alcove and able to collect water from the entire ceiling of the alcove. A seepage rate was then approximated by dividing the amounts of total seepage, collected within a given time interval (about one day), by the corresponding time interval. Tracer concentrations of seepage were obtained by analyzing the seepage water collected from each time interval. Therefore, the concentration data correspond to average values for the corresponding time intervals. The seepage rate and tracer concentration data are used for evaluating the numerical approach.

3. Modeling Schemes

3.1 Multiple interacting continua (MINC) model

A number of schemes based on the continuum approach for modeling flow and transport in unsaturated fractured rocks are available in the literature. Typical schemes include the effective-continuum model (ECM) (Pruess et al., 1990), the dual-porosity model (Warren and Root, 1963), the dual-permeability model (Robinson et al., 1997) and the multiple interacting continua (MINC) model (Pruess and Narasimhan, 1985). A recent review of these schemes was given by Doughty (1999).

Most of the continuum schemes cannot accurately consider the highly transient flow and transport between fractures and the matrix, because of the thermodynamic equilibrium assumption (in the ECM) and the use of one matrix block (in the dual-porosity and dual-permeability models) (Doughty, 1999). To overcome this problem, Pruess and Narasimham (1985) proposed the MINC model, which is similar to the dual-permeability model except that the matrix is further subdivided into several continua, depending on the distances to the fracture-matrix interface. Therefore, the MINC can more accurately resolve sharp gradients near the interface and is more suitable for modeling transient flow and transport. Considering the highly transient nature of the infiltration test, the MINC model was used, with the matrix subdivided into three matrix continua.

3.2 Active fracture model

Unsaturated flow in fractures is commonly characterized by fingering flow at different scales. This flow mechanism must be considered to accurately model flow and transport

in fractured rocks. Recently, Liu et al (1998) proposed an active fracture model to incorporate this mechanism into the continuum approach. This model was used in this study for describing flow and transport in fractures. Liu et al. (1998) divided the fracture continuum into two parts, active and inactive, to account for fingering flow at the fracture network scale. Flow and transport occurs only within the active fracture continuum, with the inactive part simply bypassed. The portion of active fracture continuum relative to the whole fracture continuum is dynamic and depends on flow conditions. This concept is generally supported by a variety of field data obtained from the unsaturated zone of Yucca Mountain (Liu et al., 1998), and the concept is also generally consistent with field observations from the infiltration test. During the early stage of the infiltration test, seepage was initially observed from one fracture on the ceiling of the alcove, and the wetting area expanded over time. Seepage rate was spatially variable, with total seepage generally coming from a small portion of the ceiling, suggesting that only a portion of the fractures was actively conducting water during the test.

Liu et al. (1998) further assumed that van Genuchten (1980) relations are approximately valid for the active fracture continuum and that the fraction of active fractures in a connected fracture network is a power function of effective fracture saturation. On the other hand, because of the fingering flow in a fracture network, not all fracture-matrix interface areas are available for flow and transport between fractures and the matrix. The ratio of the interface area contributing to the flow and transport between fractures and the matrix, to the total interface area determined geometrically from the fracture network, is called the fracture-matrix interface area reduction factor, given by (Liu et al., 1998)

$$R = S_e^{1+\gamma} \qquad (1)$$

where $\gamma < 1$ is a positive factor describing the "activity" of a connected fracture network. The effective fracture saturation (S_e) is defined as

$$Se = \frac{S_f - S_r}{1 - S_r} \qquad (2)$$

where S_f is the water saturation of all connected fractures and S_r is the residual fracture saturation. Equation (1) includes the additional effects of the difference between the active fracture spacing and the actual fracture spacing by assuming capillary pressure gradient (or concentration gradient) near the fracture-matrix interface to be inversely proportional to the active fracture spacing. A detailed derivation of the constitutive relationships for the active fracture model is given by Liu et al. (1998). Equations (1) and (2) are used to calculate flow and transport between fractures and the matrix. A larger R value generally corresponds to a smaller resistance for flow and transport between fractures and the matrix.

3.3 Numerical model for the test site

Because the MINC scheme needs substantial computational time and memory (especially for performing model calibration with inverse modeling, which involves many forward simulation runs), a simple cylindrical grid was constructed for simulating the infiltration test (Figure 2). Both fractures and matrix were treated as homogeneous continua as a result of data limitation. (A heterogeneous model or a fracture network model generally needs more data.) The grid extended 45 m in the vertical direction and

30 m in the radial direction (with a 60 m diameter). Ground surface was approximated as horizontal. Model domain was considered to be large enough, in comparison with size of the alcove and infiltration application area, such that side boundaries had an insignificant effect on flow and transport near the alcove. On the basis of the site data, a square opening representing the alcove was created in the grid 30 to 35.5 m below the ground surface. The grid was regular, with 10 cm grid spacing around the alcove and 1 m grid spacing away from the alcove.

The temporally variable inflow rates were imposed on the top boundary, representing the infiltration condition. The side boundary corresponded to a zero-flow condition in the radial direction. The alcove ceiling and wall boundary was modeled by a zero capillary-pressure condition, representing a relative humidity of 100% in the alcove (Birkholzer et al., 1999). Initial conditions for rock mass within the model domain were determined by assuming the test rock to to be solute-free and in gravity-capillary equilibrium with the lower boundary assigned a matrix saturation of 0.61, which was consistent with field observations under ambient conditions (Flint, 1998). A free-drainage condition at the lower boundary was then used for modeling flow and transport after the infiltration test was initialized.

In this study, the model calibration and prediction of seepage into the alcove used the inverse modeling code ITOUGH2 (Finsterle, 1997). Model calibration is defined herein as the adjustment of rock hydraulic parameters to make simulation results match the corresponding data. T2R3D (Wu et al., 1996) was used for tracer transport modeling. Note that T2R3D and ITOUGH2 use exactly the same numerical procedure to simulate water flow (Wu et al., 1996; Finsterle, 1997).

Rock hydraulic properties needed as inputs into the model include fracture spacing, fracture and matrix permeabilities, porosities, van Genuchten (1980) parameters, and the parameter of the active fracture model, γ. The fracture porosity and spacing were estimated from fracture map data obtained in the ESF. Fracture permeability was estimated based on air injection tests performed in the same geologic unit as that of the test site (LeCain, 1997). The van Genuchten (1980) parameters for the fracture continuum were estimated on the basis of fracture permeability and frequency data (Sonnenthal et al., 1997). The average matrix properties of the geologic unit, where the alcove is located, are given by Flint (1998). These property data are listed in Table 1.

4. Results and Discussion

4.1. Methodology for model evaluation

Before performing model prediction, we used the seepage data collected from the alcove during Phase I of the test ($t < 175$ days) for model calibration by adjusting rock parameters, including porosities, permeabilities, van Genuchten α for the fracture and matrix continua, and the active fracture parameter γ. Seepage into the alcove is generally less sensitive to other relevant parameters, such as residual saturation and van Genuchten *m*. Therefore, these parameters were fixed during the inverse modeling with ITOUGH2 to reduce the number of variables for model calibration. Model calibration was needed to provide rock parameters that could be used for model prediction, considering scales issues and uncertainties involved in initially measured or calculated rock parameter values.

Following model calibration with Phase I seepage data, seepage into the alcove was simulated for Phase II to examine the predictive capability of the model. Then, model

calibration was performed using seepage data from both Phase I and Phase II to obtain more accurate rock property estimates. Later in Phase II, a tracer, bromide, was introduced into the infiltrating water at the ground surface. The tracer concentrations of seepage water were measured during the test. Comparing the observed and simulated tracer concentrations provided another opportunity to check the usefulness of the model.

4.2. Modeling seepage into the alcove

Flow processes in unsaturated rocks at the test site are determined by several mechanisms. Liquid water applied at the ground surface is expected to flow mainly through fractures above the alcove: flow in a fracture network is dominated by gravity, and flow direction above the alcove is generally in the vertical direction. As previously discussed, fingering flow occurs at both a fracture and a fracture network scale, giving rise to liquid water flow occurring only within a portion of fracture voids (fast flow paths). This can considerably reduce flow from fractures to the matrix, although matrix imbibition can still be an important factor in retarding flow from the surface to the alcove. When water arrives at the top of the alcove, it cannot immediately seep into the alcove until the capillary pressure becomes zero at the ceiling of the alcove. This is because an underground opening, corresponding to the alcove herein, acts as a capillary barrier, diverting flow away from the opening (Philip et al., 1989; Birkholzer et al., 1999). Consequently, only a portion of water arriving at the zone near the ceiling of the alcove actually seeps into the alcove.

Figure 3 shows a comparison between Phase I seepage-rate data and the simulation result from the model calibration. Large discrepancies exist between the simulated and

observed seepage rate values at three major peaks. Although it is possible that use of the homogeneity assumption and the continuum approach underestimates the variability of seepage rates, we believe that the more likely reasons for error are the inaccuracies of the model in presenting site conditions during Phase I of the test.

First, in this study, we modeled liquid water flow with Richard's equation, which ignores vapor transport. An isothermal condition was also assumed for simplicity's sake. In reality, Phase I of the test was conducted from March to August of 1998. Temperature was high in the late stage of Phase I, which could have resulted in considerable vapor transport through highly permeable and well-connected fractures. This may explain why the third peak in the seepage rate data (Figure 3) was considerably overestimated. According to our modeling study (not shown here), the matrix saturation near the fracture-matrix interface is high, at t = 100 days, between the alcove's ceiling and ground surface, resulting in small simulated matrix imbibition between 100 and 200 days. Simulated results thus show a strong response to the infiltration pulses during this period. In reality, the vapor transport might remove a portion of the liquid water from the fracture and the matrix near the fracture-matrix interface area. This should give rise to a weaker seepage response to the infiltration, as indicated by the data (Figure 3).

Second, owing to the temporally variable infiltration rates in Phase I (Figure 1), a complex wetting and drying process was involved in both fractures and the matrix. Consequently, hysteresis might considerably affect the seepage into the alcove. However, not enough data existed for characterizing the hyteresis. Instead, the same water retention curves were used for both the wetting and drying procedures. Note that these problems

are not specific to the continuum approach; using the fracture-network approach does not avoid these problems.

Although considerable differences exist between the simulated and observed seepage rates for Phase I, some major features of the seepage, such as arrival times of peaks and valleys shown in the seepage rate data, were roughly captured by the simulation results. Thus, the rock properties determined from the model calibration with Phase I data were still used to predict seepage rates for Phase II. The predicted seepage rates for Phase II are fairly close to the observations, although the seepage rates are generally underestimated (Figure 3). To further examine whether ignoring the vapor transport is a major reason for the poor match to the Phase I data, we matched observed seepage rate peaks by adjusting the fracture α, within time intervals of 0–150 days and 400–450 days. No effort was made to match the data within the time interval of 150–400 days, during which vapor transport was considered to be important. As shown in Figure 4, a fairly good match was obtained for the peaks by simply increasing the fracture α from the calibrated value, while keeping other parameter values the same as those obtained from the model calibration. A larger fracture α corresponds to a weaker capillarity in the fracture continuum, which reduces the capillary-barrier effects of the alcove and consequently increases the seepage rates. Predicted seepage rates after 450 days match the observed rates very well when the peaks mentioned above are matched (Figure 4). This match, achieved by ignoring seepage rate data within the time interval of 150–400 days during which vapor transport was considered to be important, supports our speculation that water loss resulting from vapor transport may be a major reason for the poor match in the model calibration for Phase I. Note that vapor transport is not

considered to be important after 450 days because matrix saturation was higher, and vapor transport during the high-temperature periods can consume only relatively small portions of liquid water in the rock.

Because water loss owing to vapor transport is considered only to be an assumption, we performed a new model calibration using seepage rate data from both Phases I and II (including those collected in the time interval of 150 to 400 days) to further improve the accuracy of rock property estimates. Initial guesses for rock properties used in this model calibration are the parameter set obtained from the above data match procedure. The calibrated rock properties are generally similar for the two model calibrations (Table 1).

In summary, the results from the model calibration and prediction procedure indicate that the seepage processes can be reasonably represented by the model, considering the complexities of the problem and the simplicity of the model. The discrepancies between the simulation results and observations seem to result mainly from factors not specific to the continuum approach.

4.3. Modeling the tracer transport

The tracer was introduced into the infiltrating water from May 18, 1999–June 28, 1999, and from October 19, 1999–January 13, 2000, during Phase II of the test. The first tracer pulse introduced into the infiltrating water resulted in a very small observed concentration pulse, which corresponds to a few data points with concentrations close to the background value (Figure 5). Given this result, we focus in this paper on the test results from the second pulses introduced from October 19, 1999–January 13, 2000. Simulation results with calibrated rock properties based on Phases I and II seepage data

are presented in Figure 5 for several combinations of transport parameters, to compare with the tracer concentration data from seepage. Note that in Figure 5, zero time corresponds to the time when the tracer was initially introduced to the infiltrating water (May 18, 1999).

In the continuum approach, the advection-dispersion equation is used for describing solute transport in fracture and matrix continua. Because of the heterogeneity of fractures and the related fingering flow and transport, the longitudinal dispersivity for the fracture continuum may be very large and travel-distance dependent. Because no data were available for determining this dispersivity, we investigated the sensitivity of modeling results to the fracture dispersivity by comparing simulations with dispersivity values of 0 and 30 m (shown in Figure 5). Similar breakthrough curves were obtained for the two dispersivity values, indicating the relative insensitivity of modeling results to the dispersivity.

Figure 5 shows that simulation results are quite sensitive to parameters describing matrix diffusion, such as tortuosity for the matrix. The diffusion between fractures and the matrix (matrix diffusion) is proportional to the effective molecular diffusion coefficient, which is the product of the tracer molecular diffusion coefficient in free water and the matrix tortuosity. Because of the small pore velocity, the mechanical dispersion in the matrix was ignored in the simulations. A molecular diffusion coefficient of 2.0 x 10^{-9} m^2/s for bromide (Domenico and Schwartz, 1990) was used for predicting tracer concentration in the seepage. Directly measured matrix tortuosity data are not available for the rock matrix of the test site. Based on several studies in the literature, Francis (1997) has suggested a representative value of 0.7 for the matrix tortuosity of the Yucca

Mountain tuff. A classic formulation for calculating tortusity for porous media, τ, was given by Millington and Quirk (1961):

$$\tau = \frac{\theta^{7/3}}{\phi^2} \qquad (3)$$

where θ is the volumetric water content for the matrix and ϕ is the matrix porosity. In this study, the matrix porosity is 0.164, and typical simulated water saturation is 0.98 for the late stage of Phase II. This gives $\tau = 0.55$, on the basis of Equation (3). Therefore, we would expect the actual τ value to be between 0.5 and 0.7. Two τ values, 0.5 and 0.75, were used to model tracer transport (Figure 5). The comparison indicates that the simulated breakthrough curve is very sensitive to the effective molecular diffusion coefficient.

Considerable difference exists between the simulated and the observed tracer concentrations (Figure 5). This discrepancy can be explained by a number of factors. First, in the active fracture model, the expression for the fracture-matrix interface area reduction factor, *R*, considers the fracture spacing effect (Equation (1)). However, for the problem under consideration, matrix diffusion occurs only near the fracture-matrix interface because of the time scale; no interaction may occur between matrix diffusion processes from different fractures. In this case, the active fracture spacing has no effect on the matrix diffusion process for a given number of active fractures. As a result, the reduction factor should not consider the fracture spacing effect for this specific solute transport problem and can be given as (Liu et al., 1998)

$$R = S_e \qquad (4)$$

Equation (4) will give rise to a larger effective fracture-matrix interface area for the matrix diffusion than will Equation (1). Note that Equation (1) still holds for the water flow process because the capillary pressure distribution in the matrix is much more uniform than the solute concentration distribution for the given problem and there may be considerable interaction between fracture-matrix flow processes from nearby active fractures. Related to this issue, the interface area reduction should also be considered for interfaces between the different matrix continua, as shown in Figure 6. For simplicity, the reduction factor for an interface between the matrix continua is assumed to be the same as that calculated from (4). Note that in the previous tracer transport simulations, this interface area reduction was not considered for the different matrix continua.

Second, the total fracture-matrix interface area (A) may be different from the area given in the numerical grid (A^*), which assumes the fracture network to be represented by a set of parallel vertical fractures that exclude the effects of small-scale fractures. These small-scale fractures may not significantly contribute to the global flow, but may have a considerable effect on solute transport between fractures and the matrix. The total fracture-matrix interface area has an important effect on solute transport between fractures and the matrix. A larger interface area generally corresponds to a larger degree of matrix diffusion. We need to use a more accurate interface area for the tracer transport simulation, determined by

$$A = \beta A^* \qquad (5)$$

where β is a correction factor. Note that interface areas in Equation (5) correspond to the geometric areas between fractures and the matrix and are different from those available for flow and transport between active fractures and the matrix. The β value will be

determined by matching the observed breakthrough curve. Note that this area correction is not needed for the flow simulations. Liquid flux between fractures and the matrix is proportional to the product of the interface area and the horizontal matrix permeability. As long as the product remains the same, a change in either the interface area or the matrix permeability will not affect the liquid flux. Therefore, the effect of difference between A and A^* for flow processes has been taken into account through the calibration of matrix permeabilities. On the other hand, fracture coating may also give rise to different effective fracture-matrix interfacial areas for water flow and solute transport. Fracture coating may considerably affect water flow between fractures and the matrix, but may not significantly affect matrix diffusion (Gerke and van Genuchten, 1993)

Because of the complexity of solute transport in unsaturated fractured rocks (as discussed above), it is a challenge to match the observed breakthrough curve with the numerical simulation results. Figure 7 shows a comparison between the observations and the simulated breakthrough curve that considers all the factors discussed above. The match, obtained by adjusting the β value (Equation (7)), is fairly good. However, for $t >$ 280 days, the simulated curve underestimates the observed concentrations. One explanation is that the effective interface areas between the matrix continua are larger at the late stage owing to the nature of the diffusion process. This complex time-dependent behavior was not considered in our simulations. A larger interface area is expected to give a relatively large back-diffusion flux from the matrix to the fractures (Figure 6). This flux may result in a relatively flat breakthrough curve at later stages of the test. An alternative explanation is that a large degree of heterogeneity exists for different fracture flow and transport paths and their interaction with the matrix, which may not be

completely captured by our simple homogeneous model. Nevertheless, considering the complexity of the flow and transport problem under consideration and the simplicity of our model, the observed seepage rate and tracer concentration data are believed to be reasonably represented by our continuum-based model.

Figure 7 shows a comparison between simulation results for two β values, indicating that the simulated breakthrough curves are very sensitive to the fracture-matrix interface area, which largely determines the degree of the matrix diffusion. This sensitivity supports the findings of Bodvarsson et al. (2001). Based on a one-dimensional numerical study for the unsaturated zone of Yucca Mountain, they concluded that matrix diffusion may be a major mechanism for transport in unsaturated fractured rocks, and that dispersion in the fracture continuum may not have a significant effect on the overall transport process. Our sensitivity study result (Figure 7) also implies that inversion of the observed breakthrough curves can be a useful way to estimate the effective fracture-matrix interface area under unsaturated conditions. This point will be further investigated in our future research.

5. Conclusions

This study demonstrates that the continuum-approach-based model may be able to capture important features of the unsaturated flow and transport processes in unsaturated, densely fractured rocks, as indicated by fairly good matches between the simulated and observed results. Although more theoretical, numerical, and experimental studies are needed to provide a more conclusive evaluation, this study seems to give positive

evidence regarding the usefulness of the continuum approach in modeling flow and transport in the unsaturated fractured rocks under consideration.

It is also found that matrix diffusion may have a significant effect on overall transport behavior in unsaturated fractured rock. One potential application of this finding is to determine the effective fracture-matrix interface area by using inverse modeling to match observed tracer breakthrough curves, as proposed and preliminarily demonstrated in this study. The feasibility of this approach will be further evaluated in our future studies.

Acknowledgment. We are indebted to Max Hu, Tianfu Xu, and Dan Hawkes at Lawrence Berkeley National Laboratory for their critical and careful reviews of a preliminary version of this manuscript. We would also like to thank Dr. Rien van Genuchten at George E. Brown Jr. Salinity Lab and Dr. Hari Viswanathan at LANL for providing helpful and constructive comments on the initial version of the manuscript. This work was supported by the Director, Office of Civilian Radioactive Waste Management, U.S. Department of Energy, through Memorandum Purchase Order EA9013MC5X between Bechtel SAIC Company, LLC, and the Ernest Orlando Lawrence Berkeley National Laboratory (Berkeley Lab). The support is provided to Berkeley Lab through the U.S. Department of Energy Contract No. DE-AC03-76SF00098.

References

Bear, J., Tsang, C.F., de Marsily, G. (eds.), 1993. Flow and Contaminant Transport in Fractured Rock. San Diego, California: Academic Press.

Birkholzer, J., Li, G., Tsang, C.F., Tsang, Y., 1999. Modeling studies and analysis of seepage into drifts at Yucca Mountain. J. Contam. Hydrol., 38, 349-384.

Bodvarsson, G.S., Liu, H.H., Ahlers, R., Wu, Y.S., Sonnethal, E., 2001. Parameterization and upscaling in modeling flow and transport at Yucca Mountain. in Conceptual Models of Flow and Transport in the Fractured Vadose Zone, National Academic Press, Washington, D.C.

Domenico, P.A., Schwartz, F.W., 1990. Physical and Chemical Hydrogeology. John Wiley and Sons, New York.

Doughty, C., 1999. Investigation of conceptual and numerical approaches for evaluating moisture, gas, chemical and heat transport in fractured rock. J. Contam. Hydrol., 38, 69-106.

Finsterle, S., 1997. ITOUGH2 Command Reference, Version 3.1. Rep. LBNL-40041, Lawrence Berkeley National Laboratory, Berkeley, CA.

Flint, L.E., 1998. Characterization of Hydrogeologic Units Using Matrix Properties, Yucca Mountain, Nevada. Water Resour. Invest. Rep. 97–4243, Denver, Colorado, U.S. Geological Survey.

Francis, N.D., 1997. Memo: The base-case thermal properties for TSPA-VA modeling. Sandia National Laboratories, Albuquerque, New Mexico.

Glass, R.J., Nicholl, M.J., Tidwell, V.C., 1996. Challenging and improving conceptual models for isothermal flow in unsaturated, fractured rocks through exploration of small-scale processes. Rep. *SAND95-1824*, Sandia National Laboratories, Albuquerque, NM.

Gerke, H.H., and van Genuchten, M., 1993. A dual-porosity model for simulating preferential movement of water and solutes in structured porous media. Water Resour. Res., 29, 305-319.

LeCain, G.D., 1997, Air-injection testing in vertical boreholes in welded and non-welded tuff, Yucca Mountain, Nevada. Water Resour. Invest. Rep. 96-4262. U.S. Geological Survey, Denver, CO.

Liu, H.H., Doughty, C., Bodvarsson, G.S., 1998. An active fracture model for unsaturated flow and transport in fractured rocks. Water Resour. Res., 34 (10), 2633–2646.

Millington, R.J., Quirk, J.M., 1961. Permeability of porous solids. Trans. Faraday Soc., 57, 1200-1207.

National Research Council, 1996. Rock Fractures and Fluid Flow: Contemporary Understanding and Applications. Washington, D.C., National Academy Press.

National Research Council, 2001. Rock Fractures and Fluid Flow, Conceptual models of flow and transport in the fractured vadose zone. Washington, D.C., National Academy Press.

Philip, J.R., Knight, J.H., Waechter, R.T., 1989. Unsaturated seepage and subterranean holes: Conspectus, and exclusion problem for cylindrical cavities. Water Resour. Res., 25 (1), 16-28.

Pruess, K., Narasimhan, T.N., 1985. A practical method for modeling fluid and heat flow in fractured porous media. Soc. Pet. Eng. J., 25(1), 14-16.

Pruess, K., Wang, J.S.Y., Tsang,Y.W., 1990. On thermohydrologic conditions near high-level nuclear wastes emplaced in partially saturated fractured tuff: 2. Effective continuum approximation. Water Resour. Res., 26, 1249-1261.

Pruess, K., 1999. A mechanistic model for water seepage through thick unsaturated zones in fractured rocks of low matrix permeability. Water Resour. Res., 35 (4), 1039-1051.

Pruess, K., Faybishenko, B., Bodvarsson, G.S., 1999. Alternative concepts and approaches for modeling flow and transport in thick unsaturated zones of fractured rocks. J. Contam. Hydrol., 38, 281–322.

Robinson, B.A., Wolfsberg, A.V., Viswanathan, H.S., Bussod, G., Gable,C.W., Meijer, A., 1997. The site-scale unsaturated zone transport model of Yucca Mountain. LANL milestone report SP25BMD.

Sonnenthal, E.L., Ahlers, C.F., Bodvarsson, G.S., 1997. Fracture and fault properties for the UZ site-scale flow model. Chaper 7 of The site-scale unsaturated zone model of Yucca Mountain, Nevada, for the viability Assessmen, edited by Bodvarsson, G.S., T.M. Bandurraga, and Y.S. Wu, Rep. LBNL-40376, Lawrence Berkeley National Laboratory, Berkeley, CA.

Van Genuchten, M., 1980. A closed-form equation for predicting the hydraulic conductivity of unsaturated soil. Soil Sci. Soc. Amer. J., 44(5), 892-898.

Warren, J.E., Root, P.J., 1963. The behavior of naturally fractured reservoirs. Soc. Pet. Eng. J., 3(5), 245-255.

Wu, Y. S., Ahlers, C.F., Fraser, P., Simmons, A., Pruess,K., 1996. Software qualification of selected TOUGH2 modules. LBNL-39490, Lawrence Berkeley National Laboratory, Berkeley, CA.

Table 1. Hydrologic properties for the fracture and matrix continua

Property	**Fracture**	**Matrix**
Initial Guess, First Calibration, and Second Calibration		
Porosity (-)	0.01,0.028, and 0.03	0.164[a]
Vertical permeability (m^2)	2.29E-11, 2.90E-11, and 3.08E-11	1.2E-15, 3.64E-16 and 1.01E-15
Horizontal permeability (m^2)	2.29E-11, 3.14E-11, and 2.99E-11	1.2E-15,9.35E-16 and 3.42E-16
α (Pa^{-1})	2.37E-3, 2.07E-3, and 2.34E-3	7.12E-6, 1.84E-5 and 1.90E-5
m(-)	0.633[a]	0.346[a]
Fracture spacing (m)	0.377[a]	
Residual saturation (-)	0.01[a]	0.06[a]
γ (-)	0.15, 0.28, and 0.21	

[a]These properties are fixed during model calibrations.

Figures

Figure 1

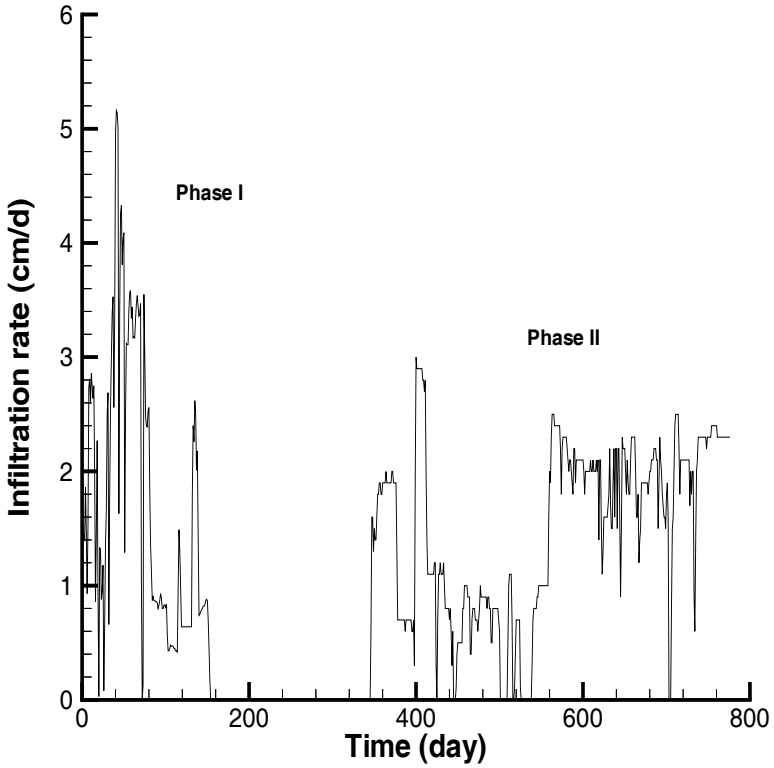
Infiltration rate (cm/d)
Time (day)
Phase I
Phase II
0
1
2
3
4
5
6
0
200
400
600
800

Figure 2

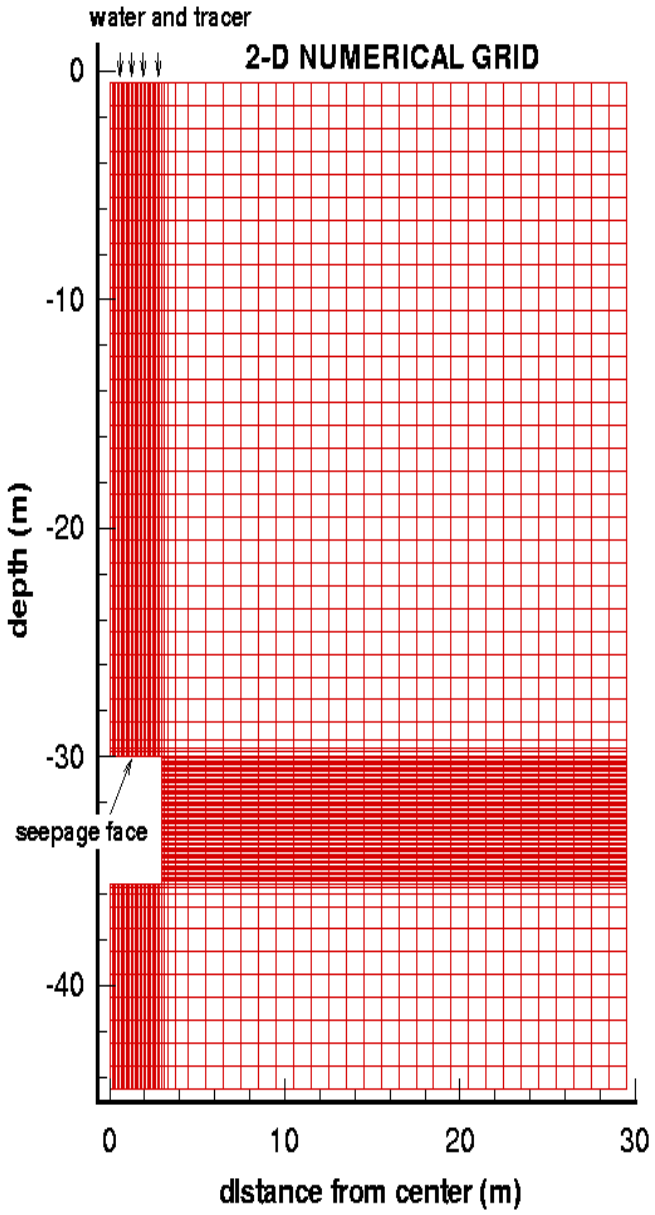
water and tracer
2-D NUMERICAL GRID
0
-10
-20
-30
-40
depth (m)
seepage face
0
10
20
30
distance from center (m)

Figure 3

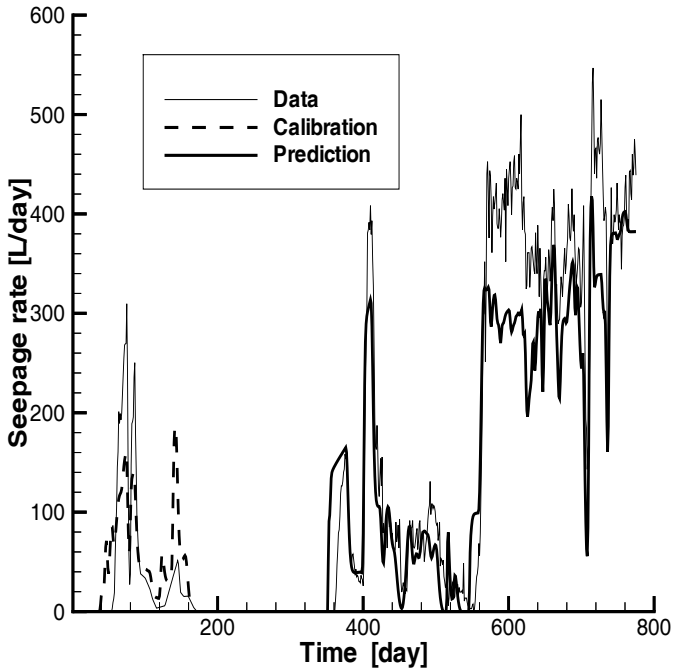
Data
Calibration
Prediction
Seepage rate [L/day]
Time [day]
0
100
200
300
400
500
600
200
400
600
800

Figure 4

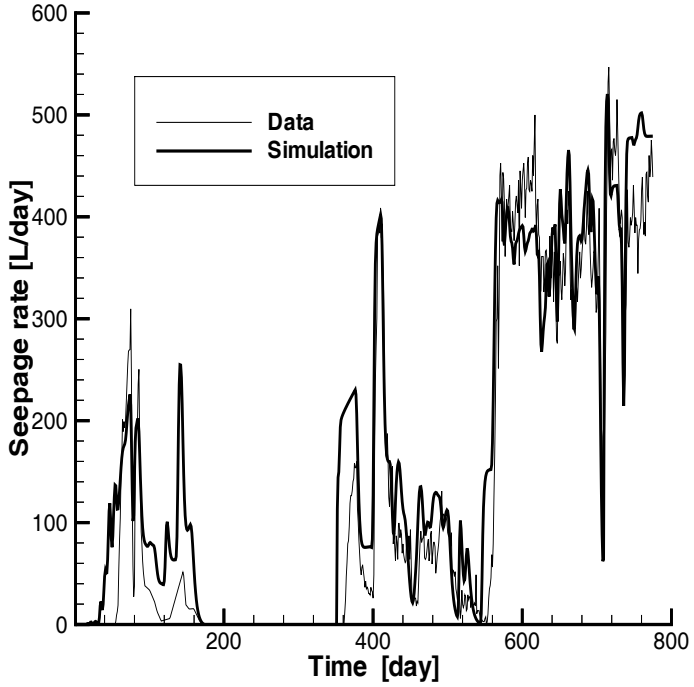
Data
Simulation
Seepage rate [L/day]
Time [day]
0
100
200
300
400
500
600
200
400
600
800

Figure 5

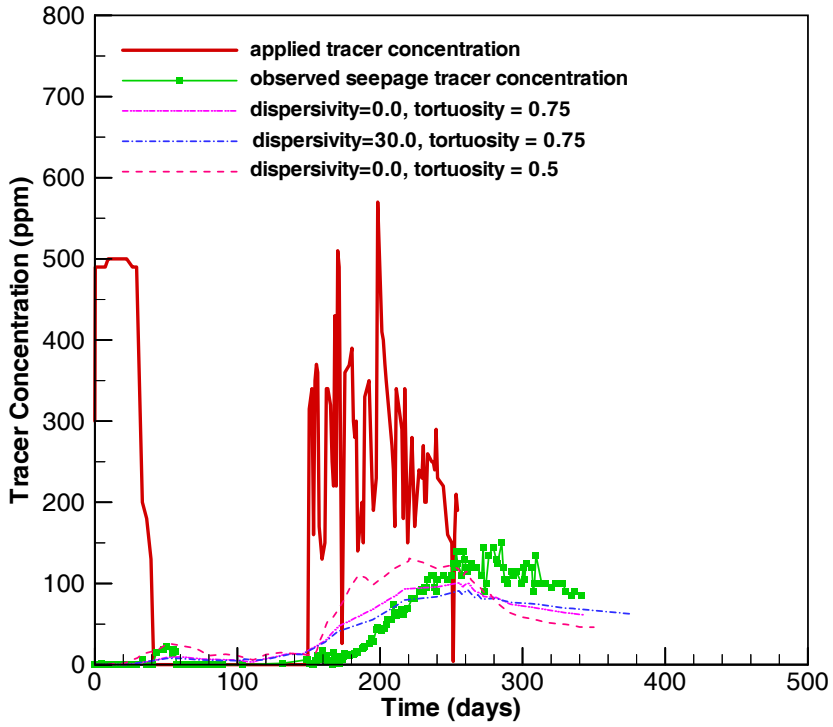
applied tracer concentration
observed seepage tracer concentration
dispersivity=0.0, tortuosity = 0.75
dispersivity=30.0, tortuosity = 0.75
dispersivity=0.0, tortuosity = 0.5
Tracer Concentration (ppm)
Time (days)
0
100
200
300
400
500
600
700
800

Figure 6

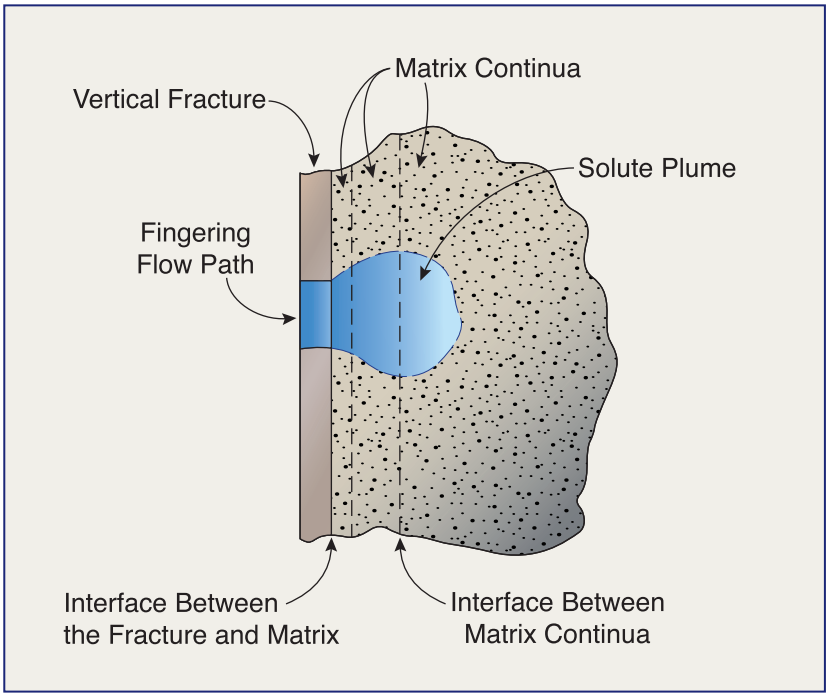
Matrix Continua
Vertical Fracture
Solute Plume
Fingering
Flow Path
Interface Between
the Fracture and Matrix
Interface Between
Matrix Continua
UZ2K168

Figure 7

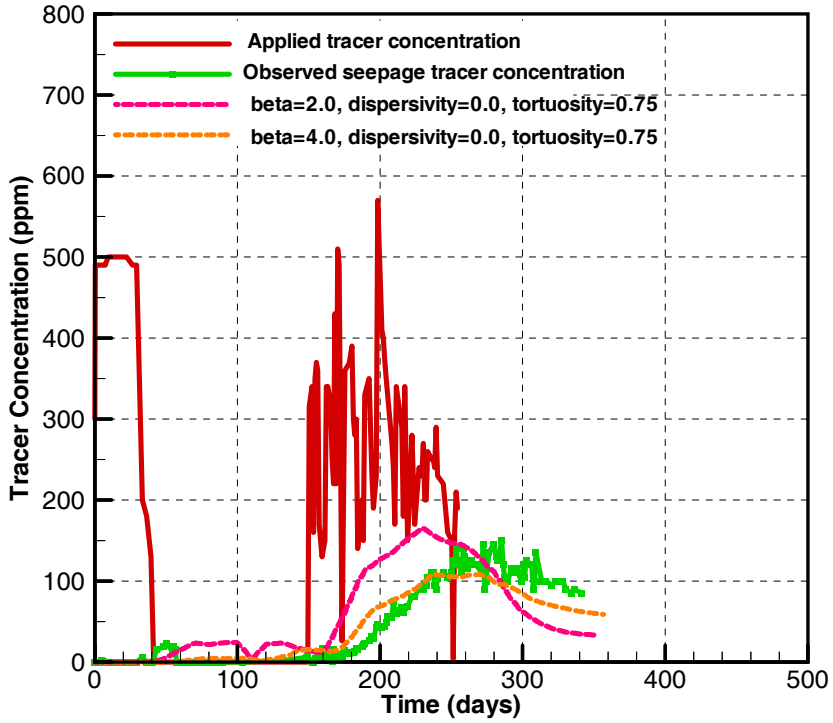
Applied tracer concentration
Observed seepage tracer concentration
beta=2.0, dispersivity=0.0, tortuosity=0.75
beta=4.0, dispersivity=0.0, tortuosity=0.75
Tracer Concentration (ppm)
Time (days)
0
100
200
300
400
500
600
700
800